Traces in ion yields and electron spectra of the formation of Ar inner-shell hollow states by free-electron lasers

A. O. G. Wallis, H. I. B. Banks, and A. Emmanouilidou
Department of Physics and Astronomy, University College London, Gower Street, London WC1E 6BT, United Kingdom
(Received 3 February 2015; published 2 June 2015)

We explore the formation of Ar hollow states with two or three inner-shell holes by free-electron-laser radiation. We find that even-charged Ar ion states can be more populated than odd-charged Ar ion states. This depends on the pulse intensity and the number of energetically accessible inner-shell holes. Fully accounting for fine structure, we demonstrate that one-electron spectra bear the imprints of Ar hollow states with two inner-shell holes. Moreover, we show how the Auger spectra of these hollow states can be extracted from two-electron coincidence spectra.

DOI: 10.1103/PhysRevA.91.063402 PACS number(s): 32.80.Fb, 32.80.Rm, 41.60.Cr, 42.50.Hz

I. INTRODUCTION

The advent of extreme-ultraviolet and x-ray free-electron lasers (FELs) allows the exploration of novel states of matter. One fascinating aspect of FELs is that the laser boils away electrons from the inside out, giving rise to hollow atoms and molecules. To monitor the femtosecond-time-scale dynamics of these hollow states one needs to identify the ionization pathways that lead to their formation. Understanding the processes leading to the formation of hollow states will allow these states to be employed as the basis for a new type of spectroscopy for chemical analysis [1–4]. It will also assist in achieving atomic resolution in diffraction patterns from biological molecules interacting with FEL radiation [5,6].

We consider Ar interacting with FEL radiation. For each additional inner-shell hole that becomes energetically accessible, a link of a P_C and an A_V transition is added to the ionization pathways. Even charged Ar ion states are primarily populated by chains of these links. P stands for a single-photon ionization of an electron and A for an Auger decay with an electron from a higher orbital, denoted as the subscript in A, dropping to fill in a hole. C and V stand for a core and a valence electron, respectively. We show that when hollow states with two inner-shell holes are formed, the ion yield of Ar^{2n+} is larger than the ion yield of $Ar^{(2n-1)+}$, with $n = 1, \ldots, h$ and h the number of holes. This is true for all intensities. However, when three inner-shell holes are energetically accessible, additional transitions become available. These are Coster-Kronig Auger (A_C) transitions [7] where the hole and the electron dropping in to fill the hole occupy subshells with the same n and different l numbers. In this case, we find that it is only for higher intensities that the yield of the even-charged Ar ion states is larger than the yield of the odd-charged Ar ion states.

Focusing on two inner-shell holes, we demonstrate how to identify the formation of the $Ar^{2+}(2p^{-2})$ hollow state [8–10]. We show that the yield of Ar^{4+}, which bears the imprint of $Ar^{2+}(2p^{-2})$, is not sufficient for identifying this hollow state. The reason is that Ar^{4+} is populated by competing ionization pathways; however, not all of these pathways contribute to the formation of the hollow state. Unlike in the ion yields, we find that in the one-electron spectra these competing pathways leave different traces and we can thus discern the formation of $Ar^{2+}(2p^{-2})$. We also show how to extract the Auger spectrum of the hollow state using FEL radiation from two-electron coincidence spectra. We note that there are several studies of Auger spectra with synchrotron radiation following, for instance, the decay of the $Ar^{+}(2p^{-1})$ [11,12] and the $Ar^{2+}(2p^{-1}v^{-1})$ [13] states.

II. RATE EQUATIONS

We first describe the rate equations we use to obtain our results [14,15]. We account for the general case when multiple states lead to state j, for example, $i \to j \to k$ and $i' \to j \to k$. To compute the contribution of the state i to the yield $\mathcal{I}_{j(i)}^{(q-1)}$ of the ion state j with charge $q-1$ we solve the rate equations

$$\begin{aligned}
\frac{d}{dt}\mathcal{I}_{j(i)}^{(q-1)}(t) &= [\sigma_{i\to j}J(t) + \Gamma_{i\to j}]\mathcal{I}_{i}^{(q-2)}(t) \\
&\quad - \sum_{k'}[\sigma_{j\to k'}J(t) + \Gamma_{j\to k'}]\mathcal{I}_{j(i)}^{(q-1)}(t), \\
\frac{d}{dt}\mathcal{P}_{j(i)\to k}^{(q)} &= \sigma_{j\to k}J(t)\mathcal{I}_{j(i)}^{(q-1)}(t), \\
\frac{d}{dt}\mathcal{A}_{j(i)\to k}^{(q)} &= \Gamma_{j\to k}\mathcal{I}_{j(i)}^{(q-1)}(t),
\end{aligned} \tag{1}$$

where $\sigma_{i\to j}$ and $\Gamma_{i\to j}$ are the single-photon absorption cross section and the Auger decay rate from the initial state i to the final state j, respectively. $J(t)$ is the photon flux, which is modeled with a Gaussian function. Atomic units are used in this work. For details on how we compute $\Gamma_{i\to j}$, see [14]. The first term in Eq. (1) accounts for the formation of the state j with charge $q-1$ through the single-photon ionization and the Auger decay of the state i with charge $q-2$. The second term in Eq. (1) accounts for the depletion of state j by single-photon ionization and Auger decay to the state k' with charge q. In addition, we compute the photoionization $\mathcal{P}_{j(i)\to k}^{(q)}$ and the Auger $\mathcal{A}_{j(i)\to k}^{(q)}$ yields, with q the charge of the final state k. These yields provide the probability for observing two electrons with energies corresponding to the transitions $i \to j$ and $j \to k$. Using these yields, we obtain the coincidence two-electron spectra. The one-electron spectra, that is, the transition yields from an initial state j with charge $q-1$ to a final state k with charge q and the ion yields of the state j and of all the

states with charge $q-1$, are given by

$$\mathcal{P}^{(q)}_{j\to k} = \sum_i \mathcal{P}^{(q)}_{j(i)\to k}, \quad \mathcal{A}^{(q)}_{j\to k} = \sum_i \mathcal{A}^{(q)}_{j(i)\to k}, \tag{2}$$

$$\mathcal{I}^{(q-1)}_{j} = \sum_i \mathcal{I}^{(q-1)}_{j(i)}, \quad \mathcal{I}^{(q-1)} = \sum_j \mathcal{I}^{(q-1)}_{j}. \tag{3}$$

III. RESULTS

A. Even- versus odd-charged Ar ion yields

In Fig. 1 we compute the yields of the Ar^{n+} ion states for four photon energies and for a high pulse intensity of 5×10^{15} W cm^{-2}. We choose a small pulse duration of 10 fs. The reason is that small pulse durations favor the $P_C P_C$ versus the $P_C A_V$ sequence, since high intensities are reached faster. The former sequence leads to an increased yield of the $Ar^{2+}(2p^{-2})$ hollow state with two inner-shell holes; this hollow state is partly the focus of the current work. Thus, in what follows all our calculations are performed with a 10 fs pulse duration. In Fig. 1 we compute the yields of the Ar^{n+}

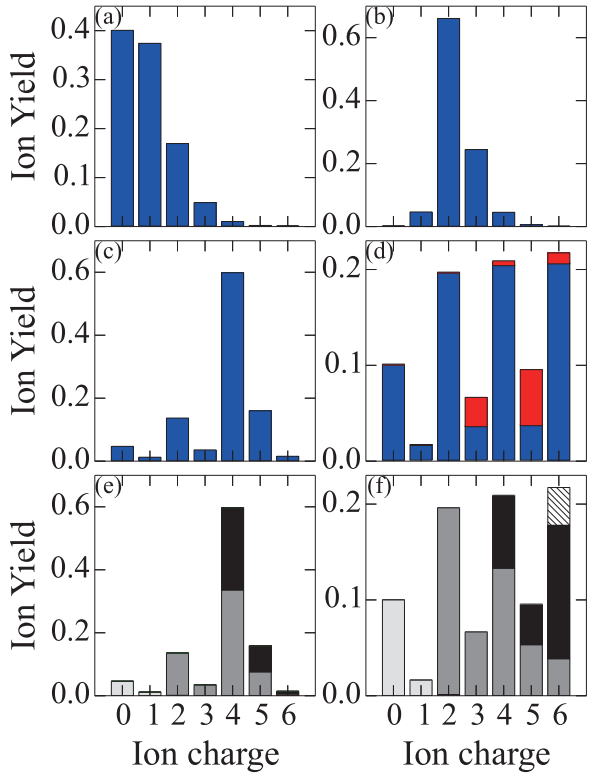

FIG. 1. (Color online) Ion yields of Ar^{n+} for a pulse of 5×10^{15} W cm^{-2} intensity, 10 fs duration, and different photon energies. For each photon energy, the number of accessible inner-shell holes is different: (a) 200 eV, no inner-shell holes; (b) 260 eV, a single $2p$ inner-shell hole; (c) 315 eV, two $2p$ inner-shell holes. (d) 360 eV, three $2p$ and a combination of two $2p$ and one $2s$ inner-shell holes. Highlighted in red is the contribution of Coster-Kronig Auger transitions. (e) for 315 eV and (f) for 360 eV show the contribution of pathways that are differentiated by the maximum number of core holes in any state along each pathway: light gray corresponds to zero maximum number of core holes, gray to one, black to two, and striped black lines to three.

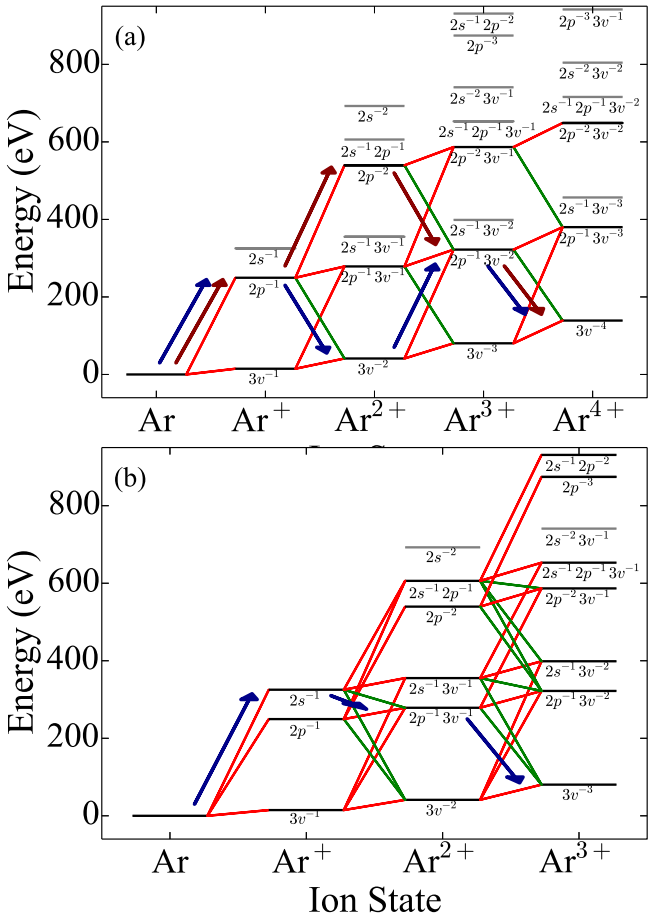

FIG. 2. (Color online) Ionization pathways between different electronic configurations of Ar accessible with P (red lines) and A (green lines) events (a) up to Ar^{4+} for $\hbar\omega = 315$ eV and (b) up to Ar^{3+} for $\hbar\omega = 360$ eV. The labels $2s^{-a}2p^{-b}3v^{-c}$ stand for the electronic configuration $(2s^{2-a}2p^{6-b}3s^{2-d}3p^{6-e})$, with $d+e=c$ the number of valence holes. In (a) $P_C A_V P_C A_V$ (blue arrows) and $P_C P_C A_V A_V$ (brown arrows) are the pathways which contribute the most to the ion yield of Ar^{4+}. In (b) the blue arrows indicate the pathway $P_C A_C A_V$ that involves a Coster-Kronig A_C transition and populates Ar^{3+}.

ion states accounting only for the electronic configuration of the ion states in the rate equations and without including fine structure [14]. We first consider a photon energy sufficiently low, 200 eV, that single-photon ionization events do not lead to the formation of inner-shell holes. In Fig. 1(a), we show that the Ar^{n+} ion states are populated in descending order. For 260 eV, a single $2p$ inner-shell hole is accessible by a P_C process from neutral Ar. A P_C is a much more likely transition than a P_V one. As a result, for all intensities, the population going through $Ar^+(2p^{-1})$ is much larger than the population ending up in or going through $Ar^+(3v^{-1})$. In addition, since the P_C photoionization is followed by an A_V decay—$P_C A_V$ pathway—the ion yield of Ar^{2+} is higher than the ion yield of Ar^+; see Fig. 1(b). For 315 eV, two $2p$ inner-shell holes are accessible by two P_C events; see Fig. 2(a). As for 260 eV, Ar^{2+} has a larger population than Ar^+. In addition, $P_C A_V P_C A_V$ and $P_C P_C A_V A_V$ are now energetically allowed pathways that populate Ar^{4+}; see Fig. 2(a). Since Ar^{3+} is populated by pathways involving at least one P_V process, Ar^{4+} has a

larger population than Ar^{3+}; see Fig. 1(c). For 360 eV, three $2p$ inner-shell holes or a combination of one $2s$ and two $2p$ inner-shell holes are accessible through three P_C events; see Fig. 2(b). Pathways involving three P_C and three A_V transitions, such as $P_C A_V P_C A_V P_C A_V$, are now energetically allowed and populate Ar^{6+}. For 200, 260, and 315 eV the odd-charged states are populated only by pathways that include at least one P_V process. In contrast, for 360 eV, pathways that include Coster-Kronig Auger transitions between the $2s$ and $2p$ subshells are energetically allowed. These pathways do not necessarily involve a P_V event. For instance, in Fig. 2(b), we show the $P_C A_C A_V$ pathway that includes a Coster-Kronig transition (A_C) and populates Ar^{3+}. When no Coster-Kronig transitions are present, the most probable pathways populating the $Ar^{(2n-1)+}$ states and those populating the $Ar^{(2n)+}$ states have the same number of P events, with $n = 1, \ldots, h$. Thus, for 260 eV and for 315 eV, the yield of the $Ar^{(2n-1)+}$ states is less than the yield of the $Ar^{(2n)+}$ states for all intensities. However, when a Coster-Kronig transition is present some of the most probable pathways populating the $Ar^{(2n-1)+}$ states have one P transition fewer than the most probable pathways populating the $Ar^{(2n)+}$ states. As a result, the yield of the $Ar^{(2n-1)+}$ states is larger (smaller) than the yield of the $Ar^{(2n)+}$ states for low (high) intensities. For a high pulse intensity of 5×10^{15} W cm^{-2}, in Fig. 1(d), we show that the ion yields of Ar^{4+} and Ar^{6+} are larger than the ion yields of Ar^{3+} and Ar^{5+}, respectively.

For the results in Fig. 1, double-ionization (DI) and double-Auger (DA) decays are not accounted for. These are both processes where two electrons are ejected in one step. Some of the pathways of DI and DA give rise to have one P process fewer compared to pathways where only one electron is ejected at each ionization step. As a result, the contribution of these two processes is less for high intensities. Moreover, these two processes are significantly less likely than the ionization processes we currently account for in our calculations. For instance, the probability for a DA decay from a $2p$ hole in Ar is roughly 10% of the probability for a single Auger decay [11].

B. Traces of double-core-hole states in the ion yields

Focusing on hollow states with two inner-shell holes, we look for observables with clear imprints of $Ar^{2+}(2p^{-2})$. We first consider the ion yields. In Fig. 3(a), for 315 eV, we plot as a function of intensity the ion yield of Ar^{4+}. We also plot the contributions to this latter yield of the $P_C P_C A_V A_V$ and of the $P_C A_V P_C A_V$ pathways and the contribution of all the remaining pathways. $Ar^{2+}(2p^{-2})$ is formed from Ar by two sequential P_C events while it is depleted through two sequential A_V events. Thus, the $P_C P_C A_V A_V$ pathway bears the imprint of the formation of $Ar^{2+}(2p^{-2})$; see Fig. 2(a). In Fig. 3(a), we also show that the yield of all other pathways that involve a P_V transition is much smaller than the yields of $P_C P_C A_V A_V$ and $P_C A_V P_C A_V$. We choose a small pulse duration, 10 fs, since it favors the contribution of the $P_C P_C A_V A_V$ pathway. However, even for this small pulse duration, the yield of $P_C P_C A_V A_V$ is similar to the yield of $P_C A_V P_C A_V$. Figure 1(e) also shows that ion yields alone do not trace the formation of $Ar^{2+}(2p^{-2})$. Indeed, pathways that go through the two-inner-shell hollow state contribute to

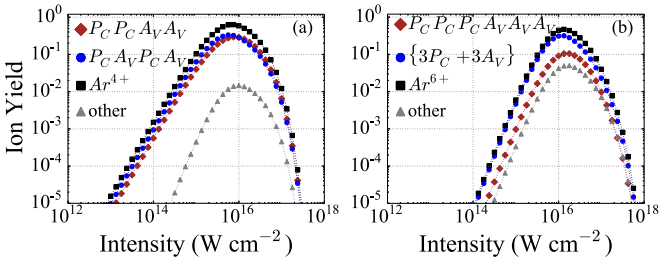

FIG. 3. (Color online) As a function of pulse intensity (a) for 315 eV and 10 fs, the ion yields of Ar^{4+} (black squares), of $P_C A_V P_C A_V$ (blue circles), of $P_C P_C A_V A_V$ (brown diamonds), and of all the other pathways contributing to Ar^{4+} (gray triangles); (b) for 360 eV and 10 fs, the ion yield of Ar^{6+} (black squares), of $P_C P_C P_C A_V A_V A_V$ (brown diamonds), of $\{3P_C + 3A_V\}$ (blue circles), and of all the other pathways contributing to Ar^{6+} (gray triangles).

the ion yield of Ar^{4+} as much as, if not less than, as pathways that go through hollow states with up to one inner-shell hole. For hollow states with three inner-shell holes, it is even more difficult to discern the pathway that bears the imprint of the hollow state. We show this to be the case for 360 eV in Fig. 3(b) where we plot as a function of intensity the yield of Ar^{6+}. We also plot the contribution to this latter yield of the $P_C P_C P_C A_V A_V A_V$ pathway, the contribution of the sum of the other $\{3P_C + 3A_V\}$ pathways that involve three P_C and three A_V events, and the contribution of all the remaining pathways. The $P_C P_C P_C A_V A_V A_V$ pathway bears the imprint of the $Ar^{3+}(2p^{-2}2s^{-1})$ and the $Ar^{3+}(2p^{-3})$ states. Its yield is smaller than the yield of the other $\{3P_C + 3A_V\}$ pathways. Also, it is only slightly larger than the sum of the yields of the pathways that involve at least one P_V process. Figure 1(f) also shows that, using ion yields alone, we cannot discern the formation of the states $Ar^{3+}(2p^{-2}2s^{-1})$ and $Ar^{3+}(2p^{-3})$. Indeed, the largest contribution to the ion yield of Ar^{6+} comes from pathways that go through states with up to two inner-shell holes.

C. One-electron spectra

We now explore whether we can identify the formation of $Ar^{2+}(2p^{-2})$ from one-electron spectra. In Fig. 4, for 315 eV, we compute the one-electron photoionization and Auger spectra for pulse parameters that optimize the contribution of the $P_C P_C A_V A_V$ pathway. Unlike for the ion yields, to accurately calculate the electron spectra we now fully account for the fine structure of the ion states in the rate equations. To obtain these fine-structure ion states we perform calculations using the GRASP2K [12] and RATIP [16] packages, within the relativistic multiconfiguration Dirac-Hartree-Fock formalism; see [14] for details. Out of all P and A transitions shown in Fig. 2(a), the most important transitions that bear the imprint of $Ar^{2+}(2p^{-2})$ are the P_C transition $Ar^{+}(2p^{-1}) \rightarrow Ar^{2+}(2p^{-2})$ and the A_V transition $Ar^{2+}(2p^{-2}) \rightarrow Ar^{3+}(2p^{-1}3v^{-2})$. Can we separate these transitions from all others in one-electron spectra?

For 315 eV, the single-photon ionized electrons from an inner shell ($2s$ or $2p$) escape with energies between 0 and 70 eV while those ionized from a valence shell ($3s$ or $3p$) escape with energy between 214 and 300 eV. The $\mathcal{P}^{(q)}_{j\rightarrow k}$

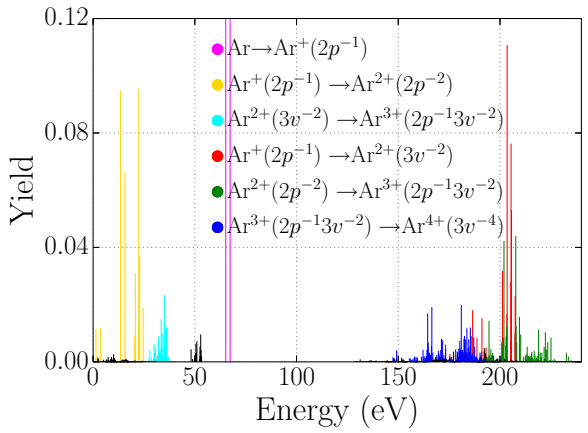

FIG. 4. (Color online) One-electron spectra, for a pulse of 5×10^{15} W cm^{-2} intensity, 10 fs duration, and 315 eV photon energy.

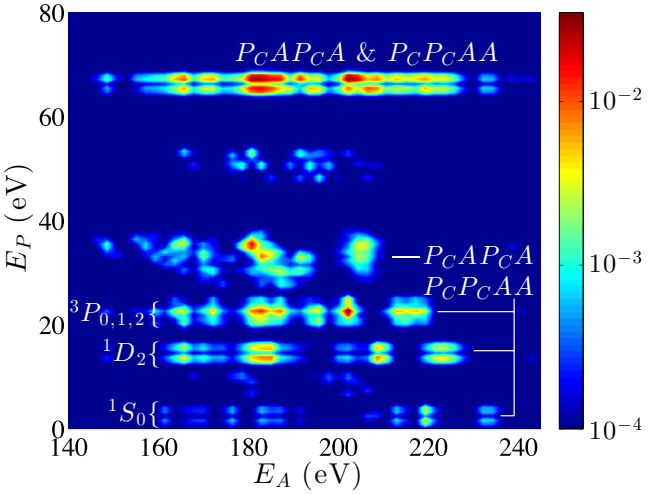

FIG. 5. (Color online) Coincidence spectra of an Auger and a photoionized electron. The pulse parameters are 5×10^{15} W cm^{-2} intensity, 10 fs duration, and 315 eV photon energy.

yields for valence-shell electrons are very small and not visible in Fig. 4. Moreover, the Auger electrons escape with energies between 150 and 240 eV. Thus, Auger electrons are well separated from single-photon ionized electrons. The most probable Auger and single-photon ionization transitions are depicted in Fig. 4. The transitions discussed in the following are depicted in Fig. 2(a). During the transitions (i) $Ar^+(2p^{-1}) \rightarrow Ar^{2+}(3v^{-2})$ the first Auger electron is ejected along $P_C A_V P_C A_V$ with energy from 173 to 208 eV [12], (ii) $Ar^{2+}(2p^{-2}) \rightarrow Ar^{3+}(2p^{-1}3v^{-2})$ the first Auger electron is ejected along $P_C P_C A_V A_V$ with energy from 181 to 241 eV, and (iii) $Ar^{3+}(2p^{-1}3v^{-2}) \rightarrow Ar^{4+}(3v^{-4})$ the second Auger electron is ejected along $P_C P_C A_V A_V$ and $P_C A_V P_C A_V$ with energy from 140 to 198 eV. Thus, the Auger transition (ii) that bears the imprint of $Ar^{2+}(2p^{-2})$ can be clearly discerned only for energies above 208 eV. For smaller energies Auger transitions (i) and (ii) strongly overlap. During the transitions (iv) $Ar \rightarrow Ar^+(2p^{-1})$ the first photoionized electron is ejected along $P_C P_C A_V A_V$ and $P_C A_V P_C A_V$ with energy from 65 to 67.5 eV, (v) $Ar^+(2p^{-1}) \rightarrow Ar^{2+}(2p^{-2})$ the second photoionized electron is ejected along $P_C P_C A_V A_V$ with energy from 1 to 25 eV, and (vi) $Ar^{2+}(3v^{-2}) \rightarrow Ar^{3+}(2p^{-1}3v^{-2})$ the second photoionized electron is ejected along $P_C A_V P_C A_V$ with energy from 22 to 41 eV. From 22 to 25 eV there is an overlap between photoionization transitions (v) and (vi). However, transition (v) is orders of magnitude larger than (vi). Since transition (v) bears the imprint of $Ar^{2+}(2p^{-2})$, we can clearly identify the formation of the hollow state from the one-electron spectra.

D. Two-electron coincidence spectra

Finally, we show how to extract the Auger spectrum of $Ar^{2+}(2p^{-2})$ from two-electron coincidence spectra. Coincidence experiments have been performed extensively with synchrotron radiation [13,17]. It is expected that coincidence experiments with FEL radiation will take place in the near future [10,18]. In anticipation of these experiments, in Fig. 5, we plot the coincidence spectra of a single-photon ionized electron and an Auger electron. This choice of electrons is based on the fact that single-photon ionized electrons are well separated in energy from Auger electrons; see Fig. 4. Moreover, we have already shown that for energies of a single-photon ionized electron (E_P) up to 25 eV we can clearly discern the second P_C event—previously denoted as transition (v)—in the $P_C P_C A_V A_V$ pathway. Indeed, as shown in Fig. 5, there is no trace of the $P_C A_V P_C A_V$ pathway for $E_P < 25$ eV. Focusing on $E_P < 25$ eV, the energies of the Auger electron from 140 to 198 eV correspond to the transition $Ar^{3+}(2p^{-1}3v^{-2}) \rightarrow Ar^{4+}(3v^{-4})$, while from 181 to 241 eV they correspond to the transition $Ar^{2+}(2p^{-2}) \rightarrow Ar^{3+}(2p^{-1}3v^{-2})$. It is this latter transition that corresponds to the Auger spectra of the $Ar^{2+}(2p^{-2})$ hollow state. In more detail, the Auger spectrum of the $^1S_0$ fine-structure state is the sum of the spectra corresponding to E_P around 1.4 and 3.6 eV. These two energies correspond to the $^2P_{3/2}$ and $^2P_{1/2}$ fine-structure states of $Ar^+(2p^{-1})$. The Auger spectrum of the $^1D_2$ fine-structure state is the sum of the spectra corresponding to E_P around 13.5 and 15.6 eV. Finally, it is more difficult to discern the Auger spectra of the $^3P_{0,1,2}$ fine-structure states in the interval $20.2 < E_P < 24.6$ eV. One reason is that some of these states differ in E_P energy by only 0.1 eV, while the uncertainty in energy from the 10 fs Gaussian pulse we use is roughly 0.2 eV. Even if a longer Gaussian pulse were used, a resolution better than 0.1 eV would be required to discern these states experimentally. In Fig. 5 the coincidence peaks have been convoluted by a 1 eV FWHM Gaussian function. Moreover, it is mainly the Auger spectra of these $^3P_{0,1,2}$ states that overlaps in the energy interval from 181 to 198 eV with the Auger transition $Ar^{3+}(2p^{-1}3v^{-2}) \rightarrow Ar^{4+}(3v^{-4})$.

IV. CONCLUSIONS

We explored how Ar states with multiple inner-shell holes affect the ion yields. We found that the ion yields of even-charged ion states are larger than the ion yields of odd-charged ion states either for all intensities or only for higher ones. This depends on the type of transitions that are energetically allowed. Our results hold for two and three inner-shell holes in

Ar. It would be interesting to further explore how our results are affected by an even larger number of inner-shell holes. Finally, motivating future FEL coincidence experiments, we demonstrated how two-electron spectra carry information regarding the Auger spectra of hollow states.

ACKNOWLEDGMENTS

A.E. acknowledges support from EPSRC under Grants No. H0031771 and No. J0171831 and use of the Legion computational resources at University College London.

[1] P. Salen *et al.*, Phys. Rev. Lett. **108**, 153003 (2012).
[2] N. Berrah *et al.*, Proc. Natl. Acad. Scis. USA **108**, 16912 (2011).
[3] R. Santra, N. V. Kryzhevoi, and L. S. Cederbaum, Phys. Rev. Lett. **103**, 013002 (2009).
[4] L. S. Cederbaum, F. Tarantelli, A. Sgamellotti, and J. Schirmer, J. Chem. Phys. **85**, 6513 (1986).
[5] R. Neutze *et al.*, Nature (London) **406**, 752 (2000).
[6] H. N. Chapman *et al.*, Nat. Phys. **2**, 839 (2006).
[7] D. Coster and R. De. L. Kronig, Physica (Utrecht) **2**, 13 (1935).
[8] L. Young *et al.*, Nature (London) **466**, 56 (2010).
[9] B. F. Murphy, L. Fang, M.-H. Chen, J. D. Bozek, E. Kukk, E. P. Kanter, M. Messerschmidt, T. Osipov, and N. Berrah, Phys. Rev. A **86**, 053423 (2012).
[10] L. J. Frasinski *et al.*, Phys. Rev. Lett. **111**, 073002 (2013).
[11] P. Lablanquie *et al.*, J. Electron Spectrosc. Relat. Phenom. **156**, 51 (2007).
[12] H. Pulkkinen *et al.*, J. Phys. B **29**, 3033 (1996).
[13] S.-M. Huttula, P. Lablanquie, L. Andric, J. Palaudoux, M. Huttula, S. Sheinerman, E. Shigemasa, Y. Hikosaka, K. Ito, and F. Penent, Phys. Rev. Lett. **110**, 113002 (2013).
[14] A. O. G. Wallis, L. Lodi, and A. Emmanouilidou, Phys. Rev. A **89**, 063417 (2014).
[15] M. G. Makris, P. Lambropoulos, and A. Mihelič, Phys. Rev. Lett. **102**, 033002 (2009).
[16] S. Fritzsche *et al.*, Comput. Phys. Commun. **183**, 1525 (2012).
[17] P. Lablanquie *et al.*, Phys. Chem. Chem. Phys. **13**, 18355 (2011).
[18] A. Rudenko *et al.*, J. Phys. B **43**, 194004 (2010).